Modélisation magnéto-thermo-hydrodynamique du soudage TIG: couplage 3D unifié de l'arc-plasma et du bain de soudage

Christopher Nahed

CSMA 2022
15ème Colloque National en Calcul des Structures
16-20 mai 2022, Presqu'île de Giens (Var)

15ème Colloque National en Calcul des Structures

Christopher Nahed[1]
[1] *CEA-Saclay, Université Paris-Saclay :* christopher.nahed@cea.fr

Résumé — Ce travail présente l'analyse des phénomènes physiques du procédé de soudage TIG (Tungsten Inert Gas), ainsi que les approches numériques utilisés pour effectuer le couplage entre l'arc-plasma et le bain de soudage. L'objectif de cette présentation est de montrer l'utilité du modèle 3D unifié développé dans Nahed [1] pour la prédiction des variables clés de soudage en fonction des paramètres procédé de base. Les simulations sont effectuées avec Cast3M [4] où des modèles de cathode, d'arc plasma et de pièce et bain de soudage sont couplés de manière robuste.
Mots clefs — Simulation multiphysique, Soudage TIG, Interactions fluides-structures, Transfert de chaleur conjugué.

1. Introduction

TIG arc welding is an ubiquitous technique used to join metallic pieces together. An arc is used to generate heat at high temperatures, allowing for the melting of the welding zone of the workpiece. In order to understand the mechanisms at play in TIG welding, the constituents of the welding system are first identified. The system is grossly made up of: an electric cathode, an arc and an electric anode. These three components serve as the electric circuit that heat the arc and turn it into a high temperature heat source. To ensure a stable and controllable electrification of the arc, the cathode is placed in a nozzle that transports a shielding gas, serving as both the electrical medium to the arc and as a protective environment (against oxidation) for the molten metal in the weld pool. The cathode is generally made of doped tungsten (with thorium or lanthanium), the arc is made of an inert gas (argon or/and helium) and the anode is the target workpiece to be welded [19]. Figure 1 schematises the above description of a typical TIG welding system. As for the technique itself, it is of particular interest to the nuclear industry due to the clean and high quality welds it produces.

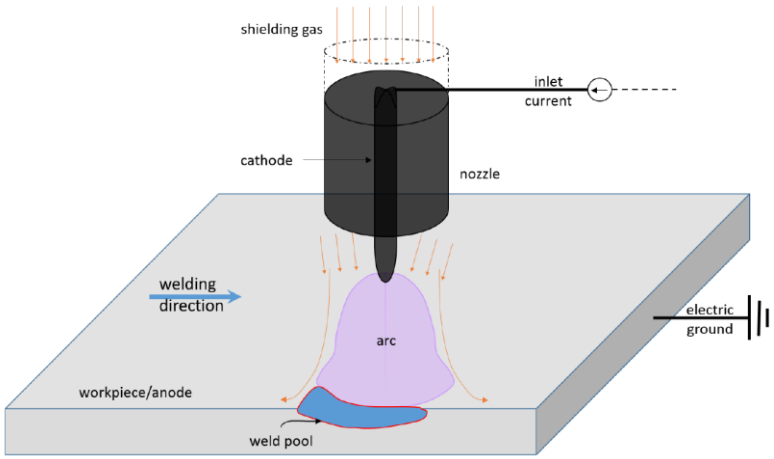

Figure 1 – Principal constituents of the TIG welding system

To understand how the metallic workpieces subject to TIG welding behave the prediction of the thermal and mechanical effects that the procedure has onto the workpiece is necessary. To this end, the magneto-thermo-hydrodynamic approach (also called the multiphysics approach) is studied and used

to create predictive models for the simulation of the welding process itself. This approach is based on the modelling of the electrodynamically forced TIG arc and its interaction with the liquid weld pool that forms in the solid workpiece. Fundamentally, this means that the efforts put into multiphysics modelling of TIG welding are to master the predictibility of the generated thermal field of the workpiece when welding. Indeed, with a predictive tool capable of accurately reproducing the thermal field from basic welding parameters, the use of experimentally calibrated thermal sources in mechanical and metallurgical studies can eventually be avoided [2,3].

2. The physical model

The following equations that are used to model the dominant physics identified in the TIG welding process are based on figure 2 seen below.

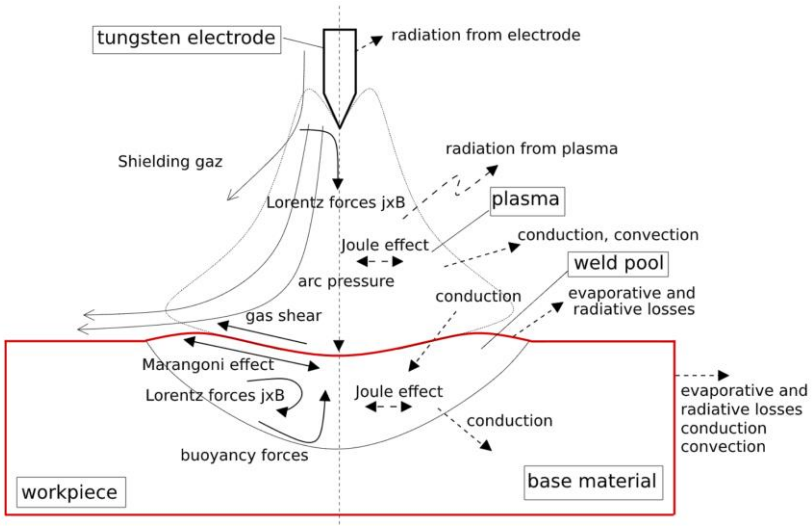

Figure 2 – Schematic of the modelled physics [2]

For the mathematical details of the physical model, the reader is referred to chapter 2 in [1]. A summary of the model is discussed below.

The used electrodynamic model respects the simplified LTE (local thermodynamic equilibrium) and continuum hypotheses. This model captures the dominant electromagnetic phenomena that occur at the mesoscopic scale. This approach allows, in a simplified manner, to calculate both the Joule effect and the Lorentz force in the TIG system. This is crucial because both the Joule effect and the Lorentz force are the dominant heat and momentum sources in the arc-plasma.

The models used for the momentum and mass conservation laws in both the arc-plasma and the weld pool allow for the resolution of the dominant fluidic effects which are important for the capture of thermal effects in the global model. Both the kinematics and dynamics at the arc-pool interface are formally derived and presented in [1], because they manifest as the dominant driving mechanisms in the pool. Therefore, ensuring that both the arc shear and Marangoni effect are properly manifest in the dynamic interface condition is paramount. Furthermore, the generalised interface conditions bring into context the importance of non-negligible advective terms that can govern the interface thermo-hydraulics if source/sink terms are added to the system.

The modelling of the energy conservation law in both the arc-plasma and the workpiece was also presented in [1] in a manner compatible with both conjugate heat transfer and phase change phenomena. Effectively, a mixed variable formulation was presented in which the temperature

variable was used for the cathode and arc-plasma model and the enthalpy variable for the workpiece model. Furthermore, the interface conditions that incorporate the equivalent electronic heat sources at the interfaces in a manner consistent with the mixed variable method were used.

3. The numerical approach

The physical model is solved using the finite element method on the Cast3M [4] toolbox. Both the Galerkin and Least Squares methods were used to approximate solutions to the physical equations. Furthermore, combinations of the Newton-Raphson and Gauss-Seidel algorithms are used to couple and solve the different physics in the global model. Figure 3 shows a schematic of the global algorithm used in this study [1].

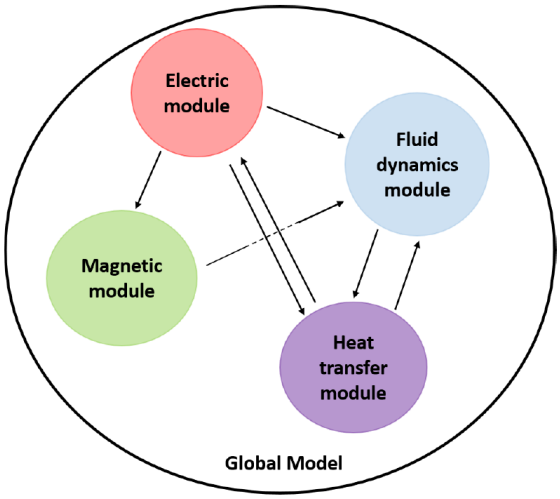

Figure 3 – Schematic of constructed modules of the global model. Each module transmits physically interpretable data in the form of velocities, temperatures, forces, fluxes etc....

For the mathematical details of the numerical methods used, the reader is referred to chapter 3 in [1]. A summary of the methods is discussed below.

The different physics modules implemented in this multiphysics TIG welding model serve to simulate the dominant phenomena as they are modelled in this study. A mix of numerical techniques and algorithms are used to look for stationary solutions to the global model. To effectively solve for stationary solutions of the TIG welding model, the physics modules represented in figure 3 are coupled in a robust global algorithm which is schematised in figure 4. Interfacing the modules is performed using Gauss-Seidel iterations while the non-linearities of each module are linearised through a quasi-Newton-Raphson approach. The thermal module couples the arc and workpiece using asymmetric Lagrange multipliers which ensures a monolithic treatment of the conjugate heat transfer and phase change model. The fluid dynamics module is solved using either a fully partitioned Dirichlet-Neumann approach or a quasi-monolithic one. The two fluid dynamics algorithms are tested in [1] for their relative performance and are coupled to a fluid interface deformation algorithm. The global algorithm is run until temperature and velocity based convergence criteria are met.

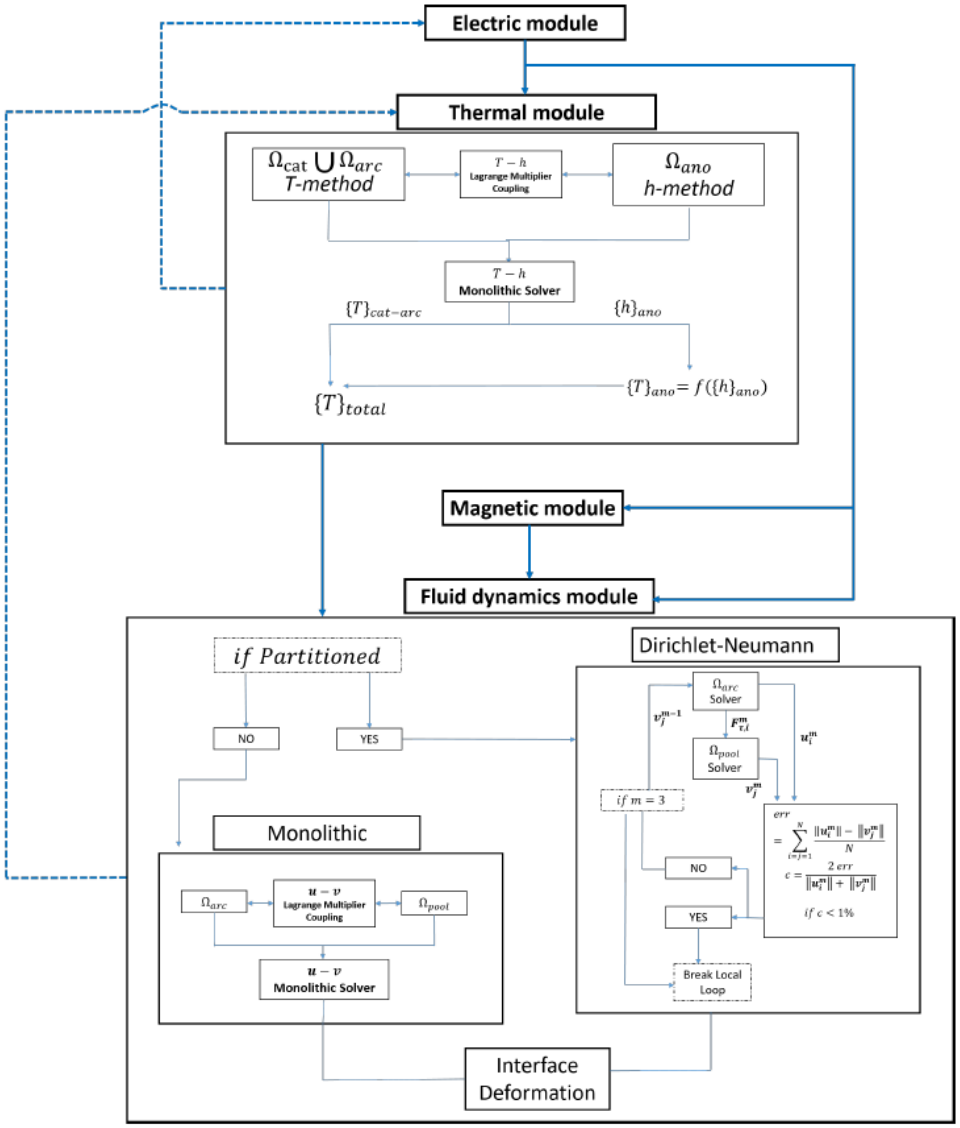

Figure 4 – Algorithm of global model. Each block represents a physics module, and the modules developed are schematised in further detail. Dashed arrows represent data flow from iteration k − 1, and the solid arrows, data from iteration k.

4. Results of the 3D TIG welding model

4.1 Computational geometry, boundary conditions and meshing

To both account for the inlet/outlet heat flux associated with the weld displacement effects and to reduce computational costs, a simplified geometric configuration is designed. The geometry is set up with both anode inlet and outlet surfaces that allow for appropriate thermal boundary conditions to be applied. Furthermore, a $z-x$ symmetry plane is assigned, which reduces the computational domain by half. The geometric configuration is schematised in figure 6.8. The workpiece thickness and arc height are chosen to correspond to the chosen experimental configuration in Koudadje's work [5]. However, the domain length and width are chosen to allow for sufficiently far inlet and exit surfaces. As seen in figure 5, the workpiece surfaces are aptly named Ω_{anoin} and Ω_{anoout}.

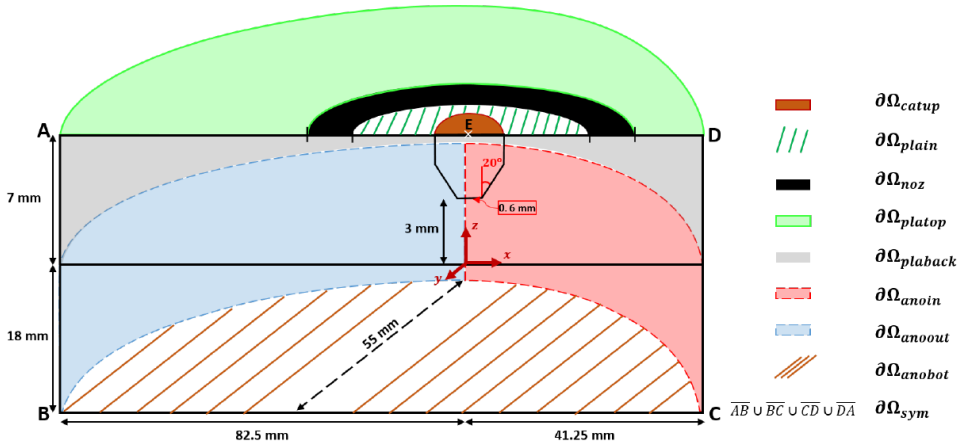

Figure 5 – Half geometry used for the simulation, sliced at the $z - x$ symmetry plane, where y = 0.

Next, the boundary conditions used to close the 3D weld displacement model, the modelled displacement effects and the mesh used to simulate the welding configuration are presented. As for the thermophysical material properties used in this simulation, they are listed in appendix A of [1]. The boundary conditions applied onto the computational domain visualised in figure 5 are presented in the table 1 below:

Electric	
$\phi = 0$	$\partial\Omega_{anobot}$
$-\sigma\nabla\phi \cdot \boldsymbol{n} = 0$	$\partial\Omega_{sym} \cup \partial\Omega_{plain} \cup \partial\Omega_{noz} \cup \partial\Omega_{platop} \cup \partial\Omega_{plaback} \cup \partial\Omega_{anoin} \cup \partial\Omega_{anoout}$
$-\sigma\nabla\phi \cdot \boldsymbol{n} = j_{\text{imp}}$	$\partial\Omega_{catup}$
Heat transfer	
$T = 500$	$\partial\Omega_{cathau} \cup \partial\Omega_{plain} \cup \partial\Omega_{noz} \cup \partial\Omega_{platop}$
$T = 300$	$\partial\Omega_{anoin}$
$-\lambda\nabla T \cdot \boldsymbol{n} = 0$	$\partial\Omega_{sym} \cup \partial\Omega_{plaback} \cup \partial\Omega_{anoout}$
$-\lambda\nabla T \cdot \boldsymbol{n} = h_{conv}(T - T_\infty)$	$\partial\Omega_{anobot}$
$-\lambda\nabla T \cdot \boldsymbol{n} = \epsilon\sigma_B(T^4 - T_\infty^4)$	$\partial\Omega_{anobot}$
Magnetic	
$\boldsymbol{B} = (0, 0, 0)$	point E
$\boldsymbol{B} = (0, —, 0)$	$\partial\Omega_{sym}$
Momentum	
$\boldsymbol{u} = (0, 0, 0)$	$\partial\Omega_{noz}$
$\boldsymbol{u} = (0, 0, —)$	$\partial\Omega_{platop}$
$\boldsymbol{u} = (—, —, 0)$	$\partial\Omega_{plaback}$
$\boldsymbol{u} = (0, 0, -1.4)$	$\partial\Omega_{plain}$
$(\boldsymbol{\sigma} \cdot \boldsymbol{n}) \cdot \boldsymbol{n} = 0$	$\partial\Omega_{platop} \cup \partial\Omega_{plaback}$
$\boldsymbol{u} = (—, 0, —)$	$\partial\Omega_{sym}$
$(\boldsymbol{\sigma} \cdot \boldsymbol{n}) = (0, —, 0)$	$\partial\Omega_{sym}$
$\boldsymbol{v} = \mathbf{V}_{displ}$	$\partial\Omega_{anoin} \cup \partial\Omega_{anoout}$

Table 1 – Boundary conditions imposed at the surfaces of schematised geometry in figure 5.

Furthermore, to account for the weld displacement effects, while respecting the stationary approach, the workpiece entry thermal field is advected using the displacement velocity w.r.t the laboratory frame of reference $\mathbf{V}_{\text{displ}}$ everywhere except inside the weld pool domain. Similarly, the weld displacement velocity is imposed as a moving rigid wall condition. This allows for a stationary solution to be found on a stationary mesh of a welding configuration undergoing displacement effects. The modelling of the weld displacement effects is schematised in figure 6 where the z − x plane of the workpiece at y = 0 is presented. Effectively, figure 6 shows that the cathode and arc domains are fixed w.r.t the laboratory frame of reference, while the workpiece is assigned the weld displacement velocity.

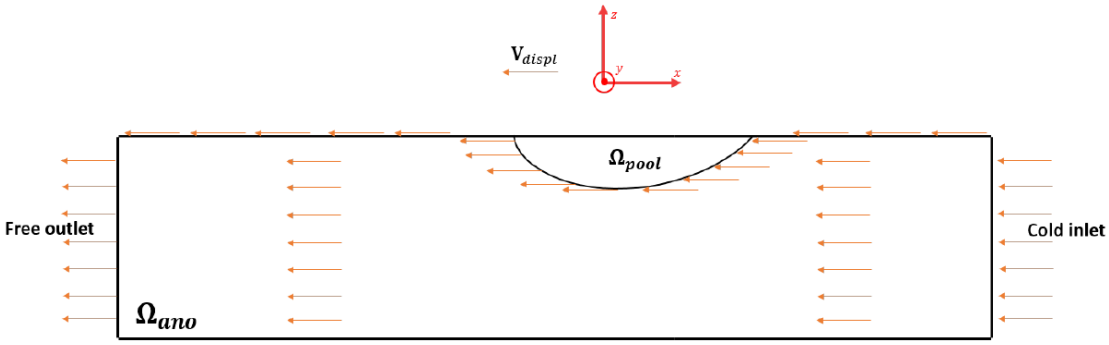

Figure 6 – Schematic of the modelled displacement effects in the workpiece.

As for the mesh generated for the simulation of the 3D welding model, its generation is schematised below in figure 7.

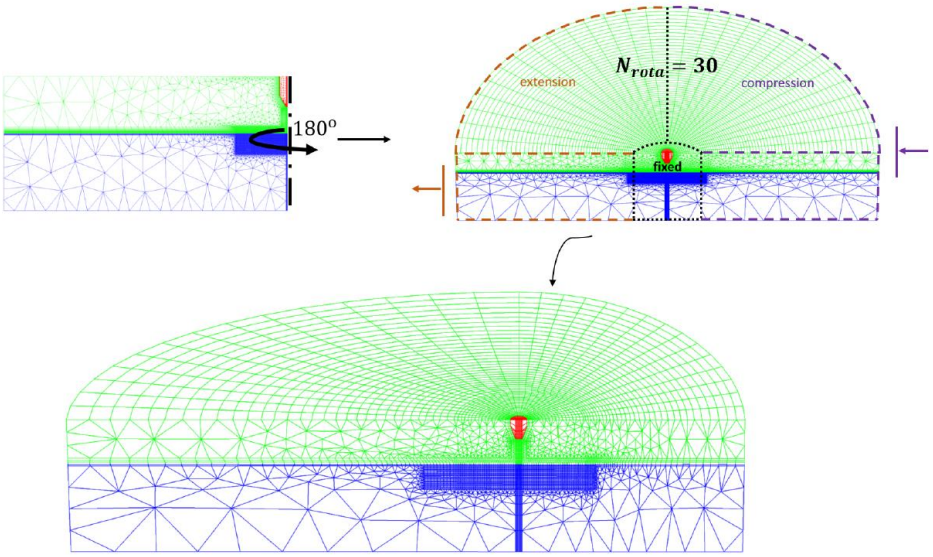

Figure 7 – Mesh generation of 3D weld displacement model by 180° rotation of 2D axisymmetric mesh and with mesh compression (front) and extension (back) effects.

4.2 Simulation results

A numerical simulation analogous to an experimental case based on Koudadje's work [5] is set up and studied. A 200 Amperes current is input through the 20° truncated cathode for a 3 mm arc that targets a 304L type steel with 10 ppm of sulfur. The weld displacement speed is 30 cm/min. The following list summarises the physical parameters used in the numerical model to simulate the case from Koudadje's work [5]:

Experimental parameters →
- $I_{arc} = 200$ A
- $H_{arc} = 3$ mm
- $\alpha = 20°$
- r_{int} = not specified
- $e_S = 10$ ppm
- $H_{ano} = 18$ mm
- $\mathbf{V}_{displ} = 30$ cm · min^{-1}
- Workpiece material → 304L

The simulation results of the 3D model (which was verified in [1]) are briefly dicussed and shown in the following. Fist, the simulated thermo-hydraulic fields in the cathode, arc-plasma and the workpiece are visualised in the superposed contour and vector plots in figure 8. The developed model is capable of effectively coupling the cathode, arc, pool and workpiece domains. The numerical approach used is shown to be robust in finding stationary solutions to 3D welding configurations that undergo displacement effects.

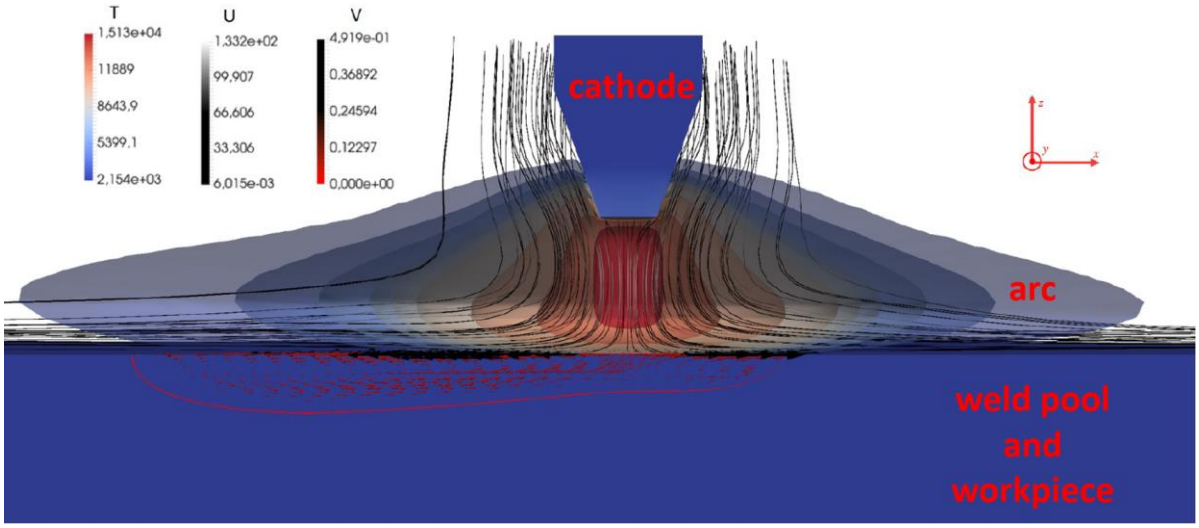

Figure 8 – Slice of the 3D global TIG domain. The temperature, arc flow and the weld pool flow are shown along with their respective scales.

The simulation results are then compared to the analogous experimental case from Koudadje [5]. The comparison is made by calculating the dimensions of the simulated weld pool and comparing them to the measured macrographic dimensions of the experimental case. The simulated weld pool and its comparison to the experimental cross section are represented in figure 9. Indeed the calculated pool depth agrees with the experimentally measured depth; however, the calculated pool width is 22% larger than the experimental one. Although the simulated welding configuration yields a pool profile that is of the same order of magnitude as the experimental cross section, identifying the sources of the discrepancy is important. The hypothesised principal sources of discrepancy are, by order of expected influence: a) the choice of the cathode upper diameter does not correspond to that reported by Koudadge [5]; b) the use of an augmented pool viscosity value; c) an underestimation of the radiative losses of the arc-plasma; d) the lack of a deformable interface in the presented simulation; e) the lack of modelling the thermal losses by contact that are present on the experimental workbench of Koudadge's work [5]. For brevity, the reader is referred to section 2 of chapter 6 in Nahed [1] for a more detailed discussion of the preliminary validation study.

5. Conclusions

The weld displacement study incorporates the cathode, arc-plasma and the workpiece domains and presents the effects of a displacement velocity onto the welding system. The developed model is a potentially powerful tool that alleviates the need for the use of experimentally calibrated heat and pressure sources. As for the calculated asymmetry in the temperature field of the arc-plasma, it implies the importance of the use of a coupled arc-plasma and workpiece model when capturing 3D displacement effects. Furthermore, the continuity of the temperature field across the API indicates that the implemented coupling algorithms remain conservative when applied to weld displacement configurations. The comparison of the numerical results to the analogous experimental case brings into context the validity of the model. The agreement between the calculated and measured pool depth

implies that the model is capable of simulating experimentally measured trends. Although an exact agreement between the simulated pool geometry and the measured dimensions is not found, the fact that the simulation results are in same the order of magnitude as the experimental measurements implies the general validity of the model. Furthermore, the calculated pool temperature and velocity fields are similar to those encountered in the literature on the numerical modelling of weld pools [2, 5].

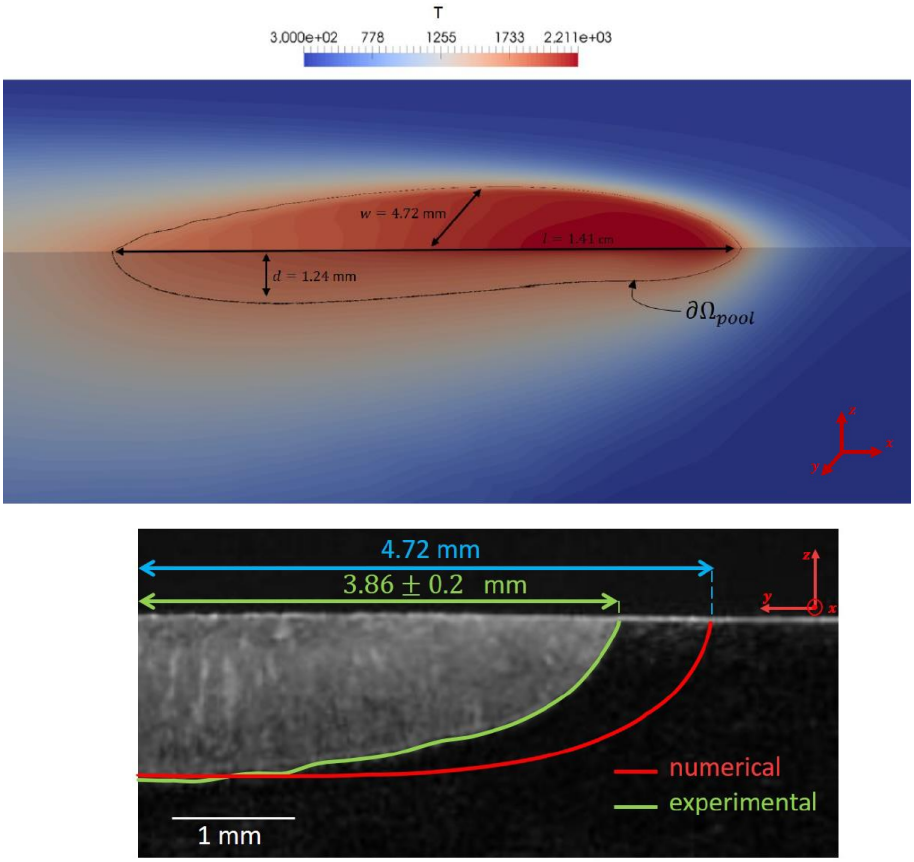

Figure 9 – Top: numerical contour of the weld pool with measured dimensions and temperature scale. Bottom: superposition of experimental macrographic cross section as taken from [5] and the simulated pool contour.

References

[1] Christopher Nahed, *Magneto-thermo-hydrodynamic modelling of TIG welding: a 3D unified coupling of the arc-plasma and the weld pool*. Doctoral dissertation, Université Aix-Marseille, November 2021.

[2] Minh-Chien Nguyen, *Modelisation et simulation multiphysique du bain de fusion en soudage à l'arc TIG.* Doctoral dissertation, Université d'Aix-Marseille, November 2015.

[3] Harry Pommier, *Stress relaxation cracking in AISI 316L-type austenitic stainless steels*. Doctoral dissertation, Ecole Nationale Supérieure des Mines de Paris, December 2015.

[4] Cast3m Web site. http://www-cast3m.cea.fr/.

[5] Koffi Koudadje, *Etude expérimentale et modélisation numérique du bain de fusion en soudage TIG d'aciers*. Doctoral dissertation, Université Aix-Marseille, 2013.